ACS Catalysis

Research Article

pubs.acs.org/acscatalysis

Origin of the Low Olefin Production over HZSM-22 and HZSM-23 Zeolites: External Acid Sites and Pore Mouth Catalysis

Fang-Fang Wei,[†] Zhi-Min Cui,[‡] Xiang-Ju Meng,[§] Chang-Yan Cao,[†] Feng-Shou Xiao,[§] and Wei-Guo Song*[,†]

[†]Beijing National Laboratory for Molecular Sciences, Laboratory for Molecular Nanostructures and Nanotechnology, Institute of Chemistry, Chinese Academy of Sciences, Beijing, 100190, People's Republic of China

[‡]School of Chemistry and Environmental Engineering, Beijing University of Aeronautics and Astronautics, Beijing, 100191, People's Republic of China

[§]Key Lab of Applied Chemistry of Zhejiang Province, Zhejiang University, Hangzhou, 310028, People's Republic of China

Supporting Information

ABSTRACT: The methanol-to-olefin (MTO) reaction was studied over two one-dimensional 10-ring zeolites with similar pore structures: ZSM-22 (TON) and ZSM-23 (MTT). It was found that the initial low but detectable production of olefins over both zeolites was catalyzed by external and/or pore mouth acid sites through hydrocarbon pool mechanism. Evidence is listed as follows: The uncalcined HZSM-22 had similar MTO activity as the calcined catalyst. The HZSM-22 zeolite with smaller crystal size had higher MTO activity. Both zeolites treated by HNO_3 to selectively leach the external acid sites showed significantly reduced initial MTO activity. Both zeolites coked through catalytic cracking of 1,3,5-triisopropylbenzene showed significantly lower initial MTO activity. This conclusion may also be suitable for other one-dimensional zeolites with pore size below 5.7 Å in the MTO reaction.

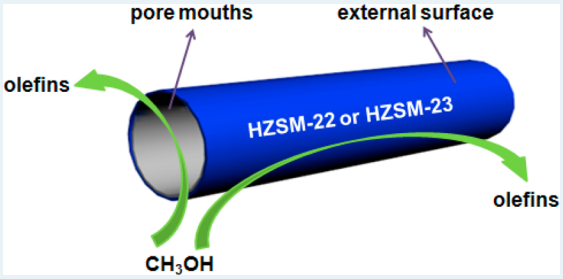

KEYWORDS: *ZSM-22 zeolite, MTO, acid treatment, coking, external surface, pore mouth catalysis*

1. INTRODUCTION

The zeolite-catalyzed conversion of methanol to hydrocarbons (MTO) has been developed into an important process for the production of C_2−C_4 light olefins from natural gas or coals. Plants with annual propene productions of 60 million tons were reported in China last year. Meanwhile, the mechanism of MTO conversion over different types of zeolites has been extensively studied, and the hydrocarbon-pool mechanism proposed by Kolboe et al. has been widely supported to explain many phenomena in the MTO process.[1−13] In the hydrocarbon pool mechanism, the methylation of the organic intermediate species (carbenium ions or methyl benzenes) and the dealkylation from the methylated intermediates are believed to be two key steps. Though exact molecular mechanisms of the latter step were still under investigation, it was safe to presume that these two steps required certain spatial spaces inside the zeolite channel, as the organic intermediates are about 1 nm in molecular size. On the other hand, however, the external and pore mouth acid sites provide enough space for the complete hydrocarbon pool cycle.

In recent years, the study of the MTO mechanism on HZSM-22 catalyst has been debated. Song et al. proposed that for HZSM-22, the hydrocarbon-pool mechanism was suppressed by its small pore size in the 10-ring one-dimensional channel (4.6 × 5.7 Å).[14−17] However, Svelle et al. and Liu et al. reported that the HZSM-22 zeolite was an active catalyst in the MTO reaction, and they believed that the olefin methylation-cracking cycle was the main reaction route of methanol conversion.[18−20] Nevertheless, one common observation was detectable olefin production over fresh HZSM-22 catalyst, and the origin of this low olefin production over ZSM-22 has yet to be clarified. According to the dual olefin and aromatic methylation catalytic cycle mechanism of Bjørgen and co-workers,[20−25] olefins could be produced from homologation and cracking of the olefins inside the channels.[15] Liu et al. believed that polymethylated aromatics coke species could be formed on the external surface or near the pore mouth which blocked the zeolite channel openings.[26] In this paper, we will provide strong evidence to demonstrate that the low initial production of olefins at the beginning of methanol flow was indeed due to the external or pore mouth acid sites.[17]

The conversion and selectivity of olefins in the MTO reactions on a microporous acidic zeolite are governed by the characteristics of the zeolite (e.g., acidity, catalyst topology, and crystallite size) and operating conditions (e.g., temperature, space velocity, and sample size).[5,27] Song et al. found dramatic activity difference between HZSM-22 and HZSM-12, which has a pore size difference of only 0.3 Å.[17] Svelle et al. recently

Received: September 25, 2013
Revised: December 20, 2013
Published: December 22, 2013

suggested that the aromatics in the channels of HZSM-22 are mostly inactive in the MTO process.[20] Ocakoglu et al. have observed pore mouth catalysis of alkane hydro-isomerization on ZSM-22.[28] Bjørgen et al. speculated that deactivation on HZSM-5 is formed on the external surface of the zeolite crystallites only.[21] Baghalha et al. elucidated that the crystal size with different external surface areas can affect the activity and selectivity of the ZSM-5 catalyst.[29] Inagaki et al. found that the ZSM-5 catalyst treated by HNO_3 has almost no acid sites on its external surfaces and can inhibit the catalytic cracking of 1,3,5-triisopropylbenzene.[30] Thus it is a rational approach to control the characteristics of the zeolites to clarify the origin of the initial olefin production on ZSM-22.

In this work, we chose ZSM-22 and ZSM-23 zeolites to study the MTO reactions. These two zeolites differed only very slightly in their pore sizes (0.46 × 0.57 nm for ZSM-22 versus 0.45 × 0.52 nm for ZSM-23). The following results were observed: The uncalcined HZSM-22 had similar MTO activity as the calcined catalyst. The HZSM-22 zeolite with a smaller crystal size had higher MTO activity. Both zeolites treated by HNO_3 to selectively leach the external acid sites showed essentially no initial MTO activity. Both zeolites covered by coke through catalytic cracking of 1,3,5-triisopropylbenzene showed significantly lower initial MTO activity. These results strongly support our conclusion that acid sites on the external acid and/or at pore mouths are the main reason for the production of olefins over HZSM-22 and HZSM-23.

2. EXPERIMENTAL SECTION

2.1. Materials and Reagents. 1,8-Diaminooctane (DAO) and 1,3,5-triisopropylbenzene (TIPB) were purchased from Acros. Colloidal silica (Ludox AS-40) was purchased from Sigma-Aldrich. Sodium aluminum oxide, aluminum sulfate $Al_2(SO_4)_3{\cdot}18H_2O$, potassium hydroxide, and HNO_3 (65−68 wt %) were purchased from Beijing Chemical Company. Methanol (UV−IR−HPLC−HPLC isocratic) was purchased from Shanghai ANPEL Scientific Instrument Co., Ltd. Pyridine (anhydrous, 99.5+%) and 2,4,6-collidine (99%) were purchased from Alfa Aesar. All chemicals were used without further purification.

2.2. Zeolite Structure. The one-dimensional 10-ring channel topologies of the zeolites are shown in Figure S1 (see Supporting Information). Their basic structural properties are summarized in Table 1.

Table 1. Summary of the Investigated Zeolites

topology	zeolite	pore topology	pore size (Å)	Si/Al[a]
TON	ZSM-22	1D, 10-ring	4.6 × 5.7	35
TON	ZSM-22-L	1D, 10-ring	4.6 × 5.7	40
MTT	ZSM-23-L	1D, 10-ring	4.5 × 5.2	20

[a]ICP analysis.

2.3. Preparation of HZSM-22. HZSM-22 with Si/Al = 45 catalysts were synthesized according to procedures in the literature,[31−33] with some modification. The molar composition of the synthesis mixture was 8.9 $K_2O/Al_2O_3/90$ $SiO_2/3$ $K_2SO_4/27.3$ DAO/3588 H_2O. The mixtures were then heated in autoclaves at 160 °C for 48 h under stirring at about 300 rpm. The samples were recovered from the autoclave, calcined at 550 °C, and ion exchanged with 1 M NH_4NO_3 solution three times at 80 °C for 12 h and then calcined at 550 °C for 8 h to obtain the proton form.

The ZSM-22-L (with Si/Al = 40) and ZSM-23-L (with Si/Al = 20) catalysts with larger crystal sizes were supplied by the Xiao group from Zhejiang University synthesized with the organic template-free method.[34]

The dealumination of calcined catalysts was carried out following the methods in the previous literature[30] by treating the calcined sample with 2.0 M HNO_3 solution (30 mL/g-sample) in a 25 mL Teflon-lined stainless-steel autoclave at 160 °C for 24 h under stirring at 300 rpm. The dealuminated samples were calcined at 550 °C for 8 h to remove NO_3^-.

2.4. Methanol-to-Olefin Reaction Test. The MTO catalytic reactions were carried out in a fixed-bed stainless-steel tubular reactor (3 mm i.d.) at atmospheric pressure. For pulse reactions, 50 mg of catalyst sample was loaded into the reactor. The reactor was preheated to 400 °C and remained at that temperature for 1 h under a 100 sccm nitrogen flow; then the reactant (5 μL) was pulsed onto the catalyst and the effluent was kept warm and analyzed by online gas chromatography. For flow reactions, methanol was fed by different velocities of N_2 flow through a bubbler containing methanol at 298 K. The GC analyses were performed after 5 min on stream under various N_2 flow rates. When there was no methanol conversion, the N_2 flow was switched back to 5 sccm to detect the gas phase products again. An Agilent 6890N GC with FID, equipped with a Supelco petrocol DH capillary column (100 m, 0.25 mm i.d., stationary phase thickness 0.5 μm) was used for the analysis.

2.5. TIPB Cracking Test. The catalytic cracking reactions of 1,3,5-triisopropylbenzene (TIPB) were carried out in the same pulse-type device with the same set up as that in the MTO reaction, except that the sample size of TIPB is 10 μL in a single pulse. Before the MTO test, the coke-covered sample was preheating at 400 °C for 8 h until no signals of TIPB as well as its cracking products were detected by GC.

2.6. Characterization. The morphology and size of the catalysts were characterized by a FESEM JEOL-6701F field-emission scanning electron microscope. XRD patterns were collected on a SHIMADZU/XRD-7000 diffractometer. The nitrogen adsorption and desorption isotherms were measured at 77 K on a Quantachrome Autosorb AS-1 instrument. The thermogravmetric analysis (TGA) was performed on a PerkinElmer/Pyris 1 TGA thermogravimetric analyzer with a heating rate of 10 °C/min under a nitrogen flow rate of 20 mL/min. The sample acidity was measured by temperature programmed desorption using ammonia as a probe molecule on a TP-5080 full-automatic adsorption instrument from Tianjin Xianquan Industry and Trade Development Co., Ltd. The samples were preheated in a 30 sccm He flow at 400 °C for 6 h. Ammonia was adsorbed for 15 min at 100 °C, and then the sample was purged by He flow to remove the physisorbed ammonia. The ammonia desorption at a heating rate of 10 °C/min up to 600 °C was monitored by a thermal conductive detector (TCD). The in situ FTIR spectroscopy experiments of adsorbed pyridine and collidine (2,4,6-trimethylpyridine) were performed on a NICOLET 6700 spectrometer and NICOLET 870, respectively. The self-supporting disk (15−20 mg) of the sample was placed in an IR cell equipped with a vacuum system and pretreated by evacuation (10^{-3} Pa) at 450 °C for 2 h. The sample disk was adsorbed pyridine at 90 °C for 1 h and then physically desorbed at 200 °C for 1 h. The collidine was adsorbed at 50 °C for 1 h, and the subsequent physical desorption was not needed.

dx.doi.org/10.1021/cs400855p | ACS Catal. 2014, 4, 529−534

3. RESULTS AND DISCUSSION

X-ray diffractograms for the three catalyst samples are shown in Figure 1. The XRD patterns of the HZSM-22 and HZSM-23-L

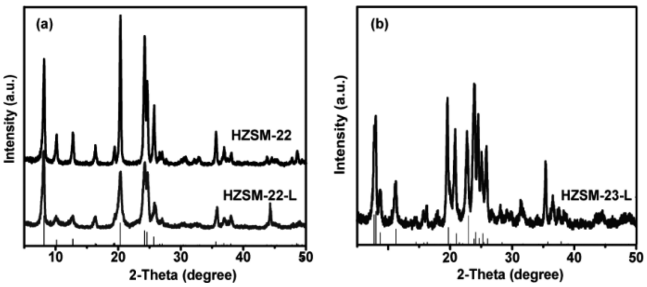

Figure 1. XRD patterns of (a) HZSM-22 and HZSM-22-L and (b) HZSM-23-L and standard reflection peaks of ZSM-22 (JCPDS 46-0569) and ZSM-23 (JCPDS 46-0570).

samples are in good agreement with their standard diffraction data, which indicated their pure crystallinity. For HZSM-22-L, a small shoulder was observed in the range 2 θ angle of 21.6–23.1. Such a shoulder might be due to the presence of a residual ZSM-5 or ZSM-11 phase.[31,33] For this study, the purity of the catalyst was important, as ZSM-5 and ZSM-11 were both excellent MTO catalysts. Even trace amounts of these two phases might account for quite significant MTO activity.

Figure 2 displays SEM images of the HZSM-22, HZSM-22-L, and HZSM-23-L catalysts. The HZSM-22 sample displays

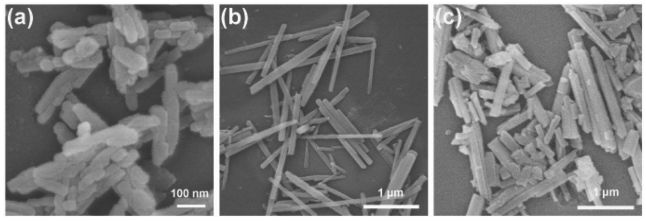

Figure 2. SEM images of (a) HZSM-22, (b) HZSM-22-L, and (c) HZSM-23-L.

needle-shaped crystals with a rough size of 300 nm × 50 nm. The HZSM-22-L was significantly larger with an average size of 1.5 μm × 70 nm. The HZSM-23-L catalyst has a slightly larger size of 2.0 μm × 130 nm.

The BET surface area of the catalysts is reported in Table 2. Nitrogen adsorption and desorption isotherms were shown in Figure S2 of the Supporting Information. For both HZSM-22 samples, since they have the same microspore structure and thus the same internal surface area, the larger BET surface area observed on the HZSM-22 sample indicated that it possessed

Table 2. BET Parameters of the Zeolite Samples

	BET (m^2/g)			
catalyst	total	external[a]	internal[b]	crystal size
HZSM-22	236	70	166	300 nm × 50 nm
HZSM-22-L	214	48	166[c]	1.5 μm × 70 nm
HZSM-23-L	120	N[d]	N[d]	2.0 μm × 130 nm

[a]Determined from sample without removal of organic template. [b]Calculated by subtracting the external surface area from the total surface area. [c]Internal surface area was the same for a certain kind of zeolite. [d]Data unavailable.

higher external surface area than the HZSM-22-L sample. This result agreed well with their crystal size difference. The HZSM-23-L has a very low BET surface area, which is accordant with the data in the literature.[35] The Si/Al ratios of the catalysts are also within a narrow range of 20–40. Thus, with these three samples, we were able to investigate the effect of pore size and external surface acid sites on their MTO activities.

In continuous flow tests, the MTO reaction was performed under different velocities of N_2 flow. All three catalysts showed some extent of MTO activity under a 5 sccm N_2 flow (WHSV = 1.33 h^{-1}; see Figure 3). The methanol conversion decreased quickly under a higher velocity of N_2 flow. In addition, when N_2 flow was switched back to 5 sccm (WHSV = 1.33 h^{-1}), the MTO activity did not recover on all three samples (see Table S1, S2, and S3 in the Supporting Information). It is unlikely that polymethylated aromatic coke species formed on the external surface or near the pore mouth[26] can block most of the zeolite channel openings within such a short reaction time. These results demonstrate that both HZSM-22 and HZSM-23 zeolites are poor MTO catalysts.

In pulse type MTO tests, all three samples showed a low but detectable production of olefins after initial methanol pulses (see GC profile in Figure S3 in the Supporting Information). Propene was the main olefin product over all three catalysts in the MTO reaction. With the same methanol dosage (5 μL) in each pulse, the intensity of propene was proportional to methanol conversion, which is very low when both methanol and dimethyl ether are regarded as the reactants. Therefore, the change of the intensity of propene against the quantity of accumulated methanol dosage was chosen to evaluate the activity of the catalysts. And when the propene peak intensity was decreased to 0.5, the catalyst was defined as MTO inactive.

HZSM-22 with a smaller crystal size was first systematically tested. Normal HZSM-22 showed low and declining propene production until methanol dosage reached 400 μL. This trend was consistent with a normal time on stream curve. Then three control samples were tested. Since there exist hardly any acid sites for zeolites with the K^+ form, and the propene production is essential zero in the MTO reaction over these three zeolites (see GC profile in Figure S4 in Supporting Information), even the uncalcined ZSM-22 sample underwent NH_4^+ exchange to obtain its H^+ form (denoted as closed HZSM-22). For the closed HZSM-22 sample, since its DAO template was not removed from the micropores, it was assumed that no MTO activity should occur inside the channel. This assumption was supported by the fact that no signals of the DAO as well as its pyrolysis products were detected during the whole heating period. The TGA curves of uncalcined HZSM-22 before and after MTO reaction have few weight losses, further demonstrating that the DAO template does not decompose under a reaction temperature of 400 °C (Figure S5 in the Supporting Information). As the channels of HZSM-22 were fully occupied by organic template agents, the production of olefins can only be generated from acid sites on the external surface. As shown in Figure 4, HZSM-22 with the DAO template showed a roughly similar initial propene production to that of the calcined HZSM-22 sample, and the propene production quickly decreased as the quantity of methanol dosage reached 80 μL. The quicker decline of the propene production than that from normal HZSM-22 was likely the lack of pore mouth catalysts on closed HZSM-22.

In order to further study the role of acid sites on the external surface and pore mouth in the MTO reaction, two methods

dx.doi.org/10.1021/cs400855p | ACS Catal. 2014, 4, 529–534

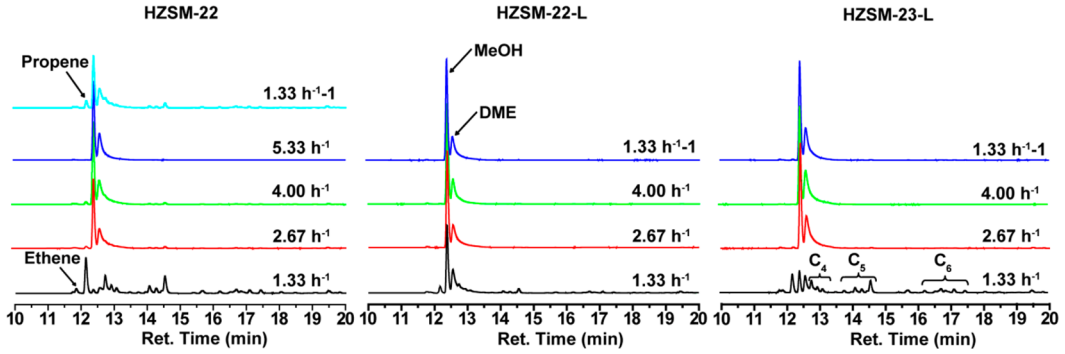

Figure 3. GC profiles of three catalysts after 5 min on-stream under different velocities of N_2 flow.

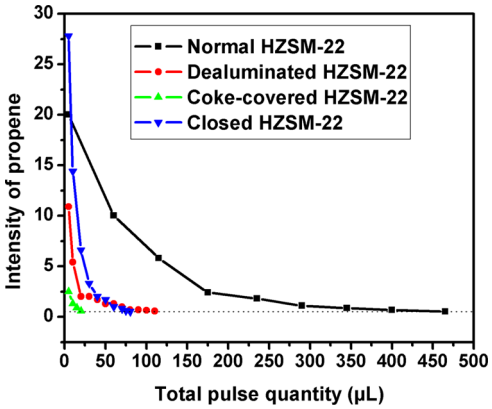

Figure 4. The intensity change of propene with quantity of methanol pulses over HZSM-22.

were applied to reduce the density of the active sites of the external surface of the HZSM-22 catalyst. One method was by HNO_3 leaching. HNO_3 leaching was able to dissolve the aluminum species near the surface of the zeolites, thus reducing the acid sites at an external surface or pore mouth. Inagaki et al. have observed similar selective dealumination of the external surfaces of MFI, TON, and MSE-type zeolites.[30] The BET surface area and micropore volume of HZSM-22 changed very little after dealumination treatment (see Table 3 and Supporting Information Figure S2), implying that the HZSM-22 has a high tolerance for HNO_3 treatment. The total amount of acid sites was reduced by 16% (see Table 3 and Supporting Information Figure S6), demonstrating that the ZSM-22 zeolite was only partially dealuminated. The FTIR spectra of common HZSM-22 and dealuminated HZSM-22 adsorbed different probe molecules are compared in Figure S7. Two peaks observed on both spectra at 3596 and 3744 cm^{-1} in Figure S7A are assigned to Brønsted acidic OH and silanol groups, respectively.[30,36] There was little change in surface hydroxy groups observed before and after acid treatment. IR spectra of adsorbed pyridine shown in Figure S7B showed a peak at 1545 cm^{-1} associated with pyridine adsorbed on a Brønsted acid site and a peak at 1489 cm^{-1} associated with adsorption on both Lewis and Brønsted acid sites, as well as a peak at 1454 cm^{-1} associated with pyridine adsorbed on a Lewis acid site.[32] It is clear that the former peaks changed very little, while the peak at 1454 cm^{-1} decreased in intensity on dealuminated HZSM-22. Therefore, it can be concluded that the acid treatment is able to etch most Lewis acid sites on or near the external surface. For the adsorption of collidine, as it is larger than the pore size of ZSM-22, it should be adsorbed only at acid sites on the external surface.[30,37,38] The peak in Figure S7C at 1638 cm^{-1} associated with collidine adsorbed on a Lewis acid site of common HZSM-22 disappeared after acid treatment, implying that acid sites at the external surface were removed after dealumination. The other two peaks at 1618 and 1574 cm^{-1} are assigned to collidine hydrogen-bonded to silanol groups. Thus, it is concluded from FTIR spectral analysis that the acid treatment of ZSM-5 zeolite developed by Inagaki et al.[30] is also working on the studied ZSM-22 samples. The corresponding catalytic result also showed significant reduction of propene production at the initial methanol pulse for dealuminated HZSM-22 compared to normal HZSM-22, as shown in Figure 4.

Table 3. Parameters of the HZSM-22 Samples before and after Treatments for Reducing the Density of the Active Sites on the External Surface and Pore Mouth

samples	BET surface area[a] (m^2/g)	micropore volume[b] (m^2/g)	amount of acid sites[c] (mmol/g)
common HZSM-22	236	0.063	0.94
dealuminated HZSM-22	210	0.061	0.79
coke-covered HZSM-22	112	0.022	0.60

[a]Determined from the nitrogen adsorption−desorption isotherm. [b]Estimated by using the t-plot method. [c]Calculated from NH_3-TPD profiles.

The other method was to selectively deposit coke on the external surface by pulsing TIPB onto the catalyst. Since TIPB was a large molecule, it was unable to diffuse into the ZSM-22 channel and could only crack at external acid sites and pore mouth sites. Coke could then form to cover the active sites on external or pore mouth active sites. The internal surface area of coke-covered HZSM-22 was 42 m^2/g, and the amount of acid sites still remained at 0.6 mmol/g (see Table 3), indicating that although a part of pore mouths are blocked, a considerable part of the internal pores of coke-covered HZSM-22 are still accessible to N_2 and NH_3 molecules. Nearly no propene was produced even at the beginning of the methanol pulses, indicating that this catalyst was unable to catalyze MTO reaction when its external and pore mouth active sites were covered by selectively deposited coke.

For frequently used zeolites such as ZSM-5 and SAPO-34, the MTO process mainly occurs in the channels rather than on external surfaces. However, for HZSM-22, its low propene production and especially the diminishing propene production on dealuminated HZSM-22 or coke-covered HZSM-22

dx.doi.org/10.1021/cs400855p | ACS Catal. 2014, 4, 529−534

strongly suggested that the observed MTO activity on HZSM-22 was due to the external acid sites or pore mouth acid sites rather than those in the internal micropores. Similar results were obtained over HZSM-22-L and HZSM-23-L samples with larger crystal sizes.

As shown in Figures 5 and 6, both HZSM-22-L and HZSM-23-L showed a similar propene production trend as HZSM-22.

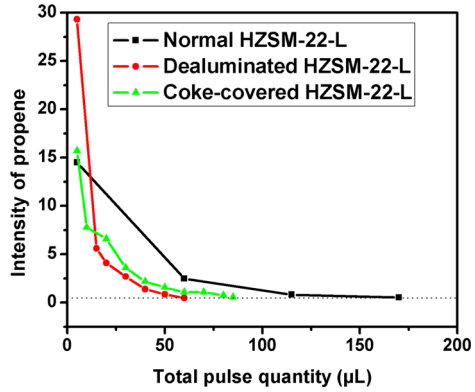

Figure 5. The intensity change of propene with the quantity of methanol pulses over HZSM-22-L.

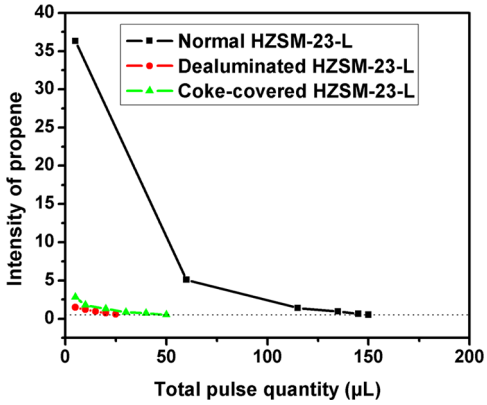

Figure 6. The intensity change of propene with the quantity of methanol pulses over HZSM-23-L.

For HZSM-23-L, the effect of reducing the external acid sites was even more significant, as dealuminated HZSM-23-L and coke-covered HZSM-23-L showed almost no production at all (see Figure 6).

Furthermore, by comparison of MTO activity among three normal acidic zeolites (see Figures 4, 5, and 6), apparently the HZSM-22 catalyst displays the best activity in the MTO reaction, which can be attributed to its smallest crystal size and highest external surface area. Reports have shown that many catalytic reactions actually take place on the external surface or at pore mouths of the crystals.[39,40] Reducing the crystal size or adding mesoporosity will expose more of the external surface or increase the number of pore mouths, leading to better catalytic performance of the zeolite.[41,42] This is another indication that the MTO activity on HZSM-22 was due to the external surface areas. Catalytic cracking of TIPB showed similar results; i.e. HZSM-22 has the highest activity and HZSM-23-L has the lowest activity (Figure S8 in the Supporting Information). These results strongly demonstrated that the olefin products were generated on the external surface or at pore mouths of all three zeolites, rather than in the channels.

4. CONCLUSIONS

In summary, one-dimensional HZSM-22 and HZSM-23-L have been chosen to study the main factor affecting the production of olefins in the MTO process. External acid sites and pore mouth catalysis play a key role in the production of olefins on both zeolites through the hydrocarbon pool mechanism. This conclusion may also be applied to study the MTO mechanism over other zeolites with one-dimensional straight channels and a pore size smaller than 5.7 Å.

■ ASSOCIATED CONTENT

Supporting Information

The channel topologies of the two zeolites (TON and MTT); nitrogen adsorption and desorption isotherms of three normal zeolites HZSM-22, closed HZSM-22 zeolite, dealuminated HZSM-22, and coke-covered HZSM-22; TGA curves of closed H-ZSM-22 obtained before and after the MTO conversion; GC profiles of the first 5 μL of methanol pulsed onto three normal catalysts; GC profiles of the first 5 μL of methanol pulsed onto three zeolite samples with K^+-form; NH_3-TPD profiles of the HZSM-22 samples before and after treatments for reducing the density of the active sites on the external surface and pore mouth; FTIR spectra of pyridine-adsorbed and collidine-adsorbed common HZSM-22 and dealuminated HZSM-22 and catalytic results of the cracking of TIPB over three normal catalysts. This material is available free of charge via the Internet at http://pubs.acs.org.

■ AUTHOR INFORMATION

Corresponding Author

*E-mail: wsong@iccas.ac.cn.

Notes

The authors declare no competing financial interest.

■ ACKNOWLEDGMENTS

We gratefully thank the National Natural Science Foundation of China (NSFC 21273244, 21333009, and 21121063) and the Chinese Academy of Sciences for financial support.

■ REFERENCES

(1) Dahl, I. M.; Kolboe, S. *Catal. Lett.* **1993**, *20*, 330.
(2) Dahl, I. M.; Kolboe, S. *J. Catal.* **1996**, *161*, 304.
(3) Song, W. G.; Haw, J. F.; Nicholas, J. B.; Heneghan, C. S. *J. Am. Chem. Soc.* **2000**, *122*, 10726.
(4) Song, W. G.; Fu, H.; Haw, J. F. *J. Am. Chem. Soc.* **2001**, *123*, 4749.
(5) Haw, J. F.; Song, W. G.; Marcus, D. M.; Nicholas, J. B. *Acc. Chem. Res.* **2003**, *36*, 317.
(6) Arstad, B.; Nicholas, J. B.; Haw, J. F. *J. Am. Chem. Soc.* **2004**, *126*, 2991.
(7) Olsbye, U.; Bjørgen, M.; Svelle, S.; Lillerud, K. P.; Kolboe, S. *Catal. Today* **2005**, *106*, 108.
(8) Arstad, B.; Kolboe, S.; Swang, O. *J. Phys. Chem. A* **2005**, *109*, 8914.
(9) Lesthaeghe, D.; Van Speybroeck, V.; Marin, G. B.; Waroquier, M. *Angew. Chem., Int. Ed.* **2006**, *45*, 1714.
(10) Marcus, D. M.; McLachlan, K. A.; Wildman, M. A.; Ehresmann, J. O.; Kletnieks, P. W.; Haw, J. F. *Angew. Chem., Int. Ed.* **2005**, *45*, 3133.
(11) Svelle, S.; Joensen, F.; Nerlov, J.; Olsbye, U.; Lillerud, K. P.; Kolboe, S.; Bjørgen, M. *J. Am. Chem. Soc.* **2006**, *128*, 14770.
(12) Lesthaeghe, D.; De Sterck, B.; Van Speybroeck, V.; Marin, G. B.; Waroquier, M. *Angew. Chem., Int. Ed.* **2007**, *46*, 1311.

(13) McCann, D. M.; Lesthaeghe, D.; Kletnieks, P. W.; Guenther, D. R.; Hayman, M. J.; Van Speybroeck, V.; Waroquier, M.; Haw, J. F. *Angew. Chem., Int. Ed.* **2008**, *47*, 5179.
(14) Cui, Z. M.; Liu, Q.; Song, W. G.; Wan, L. J. *Angew. Chem., Int. Ed.* **2006**, *45*, 6512.
(15) Cui, Z. M.; Liu, Q.; Ma, Z.; Bian, S. W.; Song, W. G. *J. Catal.* **2008**, *258*, 83.
(16) Cui, Z. M.; Liu, Q.; Bain, S. W.; Ma, Z.; Song, W. G. *J. Phys. Chem. C* **2008**, *112*, 2685.
(17) Wang, Q.; Cui, Z. M.; Cao, C. Y.; Song, W. G. *J. Phys. Chem. C* **2011**, *115*, 24987.
(18) Teketel, S.; Svelle, S.; Lillerud, K. P.; Olsbye, U. *ChemCatChem* **2009**, *1*, 78.
(19) Li, J. Z.; Wei, Y. X.; Liu, G. Y.; Qi, Y.; Tian, P.; Li, B.; He, Y. L.; Liu, Z. M. *Catal. Today* **2011**, *171*, 221.
(20) Teketel, S.; Olsbye, U.; Lillerud, K. P.; Beato, P.; Svelle, S. *Microporous Mesoporous Mater.* **2010**, *136*, 33.
(21) Bjorgen, M.; Svelle, S.; Joensen, F.; Nerlov, J.; Kolboe, S.; Bonino, F.; Palumbo, L.; Bordiga, S.; Olsbye, U. *J. Catal.* **2007**, *249*, 195.
(22) Bjørgen, M.; Joensen, F.; Lillerud, K. P.; Olsbye, U.; Svelle, S. *Catal. Today* **2009**, *142*, 90.
(23) Svelle, S.; Joensen, F.; Nerlov, J.; Olsbye, U.; Lillerud, K. P.; Kolboe, S.; Bjørgen, M. *J. Am. Chem. Soc.* **2006**, *128*, 14770.
(24) Olsbye, U.; Svelle, S.; Bjorgen, M.; Beato, P.; Janssens, T. V.; Joensen, F.; Bordiga, S.; Lillerud, K. P. *Angew. Chem., Int. Ed.* **2012**, *51*, 5819.
(25) Teketel, S.; Svelle, S.; Lillerud, K.-P.; Olsbye, U. *ChemCatChem* **2009**, *1*, 81.
(26) Li, J. Z.; Wei, Y. X.; Qi, Y.; Tian, P.; Li, B.; He, Y. L.; Chang, F. X.; Sun, X. D.; Liu, Z. M. *Catal. Today* **2011**, *164*, 288.
(27) Chen, D.; Moljord, K.; Fuglerud, T.; Holmen, A. *Microporous Mesoporous Mater.* **1999**, *29*, 191.
(28) Ocakoglu, R. A.; Denayer, J. F. M.; Marin, G. B.; Martens, J. A.; Baron, G. V. *J. Phys. Chem. B* **2003**, *107*, 398.
(29) Firoozi, M.; Baghalha, M.; Asadi, M. *Catal. Commun.* **2009**, *10*, 1582.
(30) Inagaki, S.; Shinoda, S.; Kaneko, Y.; Takechi, K.; Komatsu, R.; Tsuboi, Y.; Yamazaki, H.; Kondo, J. N.; Kubota, Y. *ACS Catal.* **2013**, *3*, 74.
(31) Valyocsik, E. W. U.S. Patent 4902406, 1990.
(32) Byggningsbacka, R.; Lindfors, L. E.; Kumar, N. *Eng. Chem. Res.* **1997**, *36*, 2990.
(33) Masih, D.; Kobayashi, T.; Baba, T. *Chem. Commun.* **2007**, 3303.
(34) Wang, Y. Q.; Wang, X.; Wu, Q. M.; Meng, X. J.; Jin, Y. Y.; Zhou, X. Z.; Xiao, F. S. *Catal. Today* **2013**, in press.
(35) Teketel, S.; Skistad, W.; Benard, S.; Olsbye, U.; Lillerud, K. P.; Beato, P.; Svelle, S. *ACS Catal.* **2011**, *2*, 26.
(36) Jacobs, P. A.; Von Ballmoos, R. *J. Phys. Chem.* **1982**, *86*, 3050.
(37) Holm, M. S.; Svelle, S.; Joensen, F.; Beato, P.; Christensen, C. H.; Bordiga, S.; Bjørgen, M. *Appl. Catal., A* **2009**, *356*, 23.
(38) Thibault-Starzyk, F.; Vimont, A.; Gilson, J. P. *Catal. Today* **2001**, *70*, 227.
(39) Martens, J. A.; Souverijns, W.; Verrelst, W.; Parton, R.; Froment, G. F.; Jacobs, P. A. *Angew. Chem., Int. Ed. Engl.* **1995**, *34*, 2528.
(40) Mintova, S.; Gilson, J. P.; Valtchev, V. *Nanoscale* **2013**, *5*, 6693.
(41) Degnan, T. F. *J. Catal.* **2003**, *216*, 32.
(42) Martens, J. A.; Verboekend, D.; Thomas, K.; Vanbutsele, G.; Gilson, J. P.; Pérez Ramírez, J. *ChemSusChem* **2013**, *6*, 421.